Journal of Materials Chemistry B

Soft, flexible conductivity sensors for ocean salinity monitoring

Journal:	*Journal of Materials Chemistry B*
Manuscript ID	TB-ART-05-2023-001167
Article Type:	Paper
Date Submitted by the Author:	22-May-2023
Complete List of Authors:	Lu, Shao-Hao; University of Connecticut, Department of Materials Science and Engineering Li, Yi; University of Connecticut, Materials Science and Engineering Wang, Xueju; University of Connecticut, Materials Science and Engineering

SCHOLARONE™
Manuscripts

Soft, flexible conductivity sensors for ocean salinity monitoring

Shao-Hao Lu [a], Yi Li [a], Xueju Wang [a,b*]

[a] Department of Materials Science and Engineering, University of Connecticut, Storrs, CT 06269, USA

[b] Institute of Materials Science, University of Connecticut, Storrs, CT 06269, USA

* Email: xueju.wang@uconn.edu

Abstract

Flexible electrochemical sensors that measure the concentrations of specific analytes (e.g., ions, molecules, and microorganisms) provide valuable information for medical diagnosis, personal health care, and environmental monitoring. However, the conductive electrodes of such sensors need to be exposed to the surroundings and are usually in direct contact with chloride-containing aqueous solutions during their operation, where chloride ions (Cl^-) can potentially cause corrosion and dissolution of the sensors, negatively impacting their performance and durability. In this work, we develop soft, flexible conductivity sensors made of gold (Au) electrodes and systematically study their electrochemical behavior in sodium chloride (NaCl) solution to prevent chloride-induced corrosion and enhance their sensitivity for marine environment monitoring. The causes of gold chlorination reactions and polarization effects are identified and effectively prevented by analyzing the effects of direct current (DC) and alternating current (AC) potentials, AC frequencies, and exposed sensing areas of the salinity sensors. Accordingly, a performance diagram is constructed to provide guidance for the selection of operation parameters for the salinity sensor. We also convert the varying impedance values of salinity sensors at different salinity levels into output voltage signals using a voltage divider circuit with an AC voltage (0.6 V) source. The results offer an assessment of the accuracy and response time of the salinity sensors, as well as their potential integration with data transmission components for real-time ocean monitoring devices. This study has important implications for the development of soft, flexible electrochemical sensors that can operate efficiently in diverse biological fluids and environmental water systems.

1. Introduction

Flexible electronics is an emerging field that holds the potential to revolutionize a wide range of technologies, including wearable devices,[1, 2] medical diagnosis,[3-6] and consumer electronics.[7] Wearable and implantable electrochemical sensors are flexible electronic devices designed to measure the concentrations of specific analytes (e.g., ions, molecules, and microorganisms) in the environment.[8-11] Their sensing mechanism is based on the principles of electrochemistry, where the interaction (or reaction) between the sensing surface and the chemical/biochemical substances is quantified by applying electrical potential/current to electrodes and detecting corresponding electrical signals. Thus, a common feature of electrochemical sensors is that their sensing electrodes are exposed to the surrounding environments,[11-13] like the frequently used chloride-containing aqueous solutions, during operation. For example, biosensors are tested in phosphate-buffered saline (PBS) solutions[8, 11, 14-20] or biological fluids, such as sweat,[10, 20-23] tear,[5, 18] saliva[24, 25] and interstitial fluids.[9, 26] Additionally, electrochemical sensors for environmental monitoring and analysis are immersed in seawater,[27-30] tap water,[31] and moisten soil specimens.[32] Among various conductive materials for electrochemical sensors, including carbon-based materials, metal nanomaterials and conductive polymers, noble metals such as Au, silver (Ag) and platinum (Pt) are versatile electrode materials due to their high electrical conductivity and superior chemical stability.[33] However, the exposed sensing area of the metallic electrodes for electrochemical sensors in direct contact with the chloride ions (Cl^-) can potentially cause the dissolution of the sensors due to chlorination reactions.[34, 35] Such reaction may negatively impact the performance and durability of the sensors, and, therefore, addressing this issue is critical for the accuracy of the measurements.

Take the salinity sensor as an example, commercial salinity meters typically use stainless-steel electrodes that are passive to corrosive environments, but their rigidity limits their applications in flexible electrochemical sensors. Although metal nano-thin films are commonly utilized in flexible electronics, stainless-steel thin films have primarily been deposited onto rigid metallic substrates (hundreds of micrometers thick), which still limits their flexibility.[36] Apart from stainless-steel materials, a flexible conductivity cell with gold thin-film (Au, 100 nm) electrodes for salinity measurements has been reported.[29]. However, the study showed that the Au electrodes suffered damage when performing measurements in a NaCl solution with an alternating current (AC) of 1 mA.[29] In addition, our recent work showed that salinity sensors made of Au electrodes can function under high hydrostatic pressure of up to 15 MPa, but experienced damage when operated at a constant current of 1 μA.[37] To overcome chlorination-induced corrosion problems in salinity sensors, some researchers explored the use of carbon-based electrodes, such as laser-induced graphene (LIG) on a polyimide substrate, as an alternative material for flexible salinity sensors.[29, 38] Nevertheless, bending the LIG conductivity sensor causes the stretching of its porous graphene structure, which increases the sensing area exposed to the saline solution and leads to a transconductance rise of over 50% at the same salinity level.[29]

In this work, we perform a systematic study on the electrochemical behavior of Au electrodes in sodium chloride (NaCl) solutions to reveal the cause of the gold chlorination reactions and enhance the performance of soft salinity sensors for ocean environment monitoring. Au thin films are chosen as the model material system for this study because of their biocompatibility, chemical inertness, and long-term stability. First, direct current (DC) signals with various potentials are applied to investigate the interaction between the Au electrodes and Cl^-, and a critical potential of ≤0.8 V is identified to prevent chlorination reactions. Next, various testing parameters, including AC frequencies, AC potentials, and the exposed sensing area of the salinity sensors, are systematically and thoroughly analyzed to optimize the performance of the sensor, leading to a performance diagram that can provide important guidance for the operation of the salinity sensor. Finally, to achieve real-time salinity measurement, we utilize an AC voltage source (square wave, 0.6 V, 1 kHz) and a voltage divider circuit to convert the varied impedance values of salinity sensors at different salinity levels into output voltages. The accuracy and response time are evaluated by recording time-dependent output voltages as the salinity levels vary, which can assess the viability of integrating the developed soft salinity sensor into fully functional electronic systems.

2. Results and Discussion

Design concept of soft, flexible salinity sensors for ocean monitoring

Soft, flexible ocean sensors can enable conformal integration onto various platforms, such as marine creatures and soft robots, and realize real-time marine environment monitoring. As shown in **Figure 1**, our flexible salinity sensor comprises of two separated Au electrodes that are fabricated by depositing Au thin films (thickness of 100 nm) onto a soft substrate of bi-layer parylene C (5 μm) and polyimide (PI, 7.6 μm) using magnetron sputtering, and patterning of the Au into desired geometries (dimensions of 4 mm x 4 mm) via photolithography. A chromium thin film (Cr, 10 nm) serves as an adhesion layer between Au and parylene C. Encapsulating the sensor with a 5 μm-thick layer of parylene C from the top followed by reactive ion etching defines exposed areas on the Au electrodes and enables the protection of the parylene C-covered regions from potentially corrosive environment. As shown in the exploded view of the salinity sensor (**Figure 1**), there are four exposed areas of the two Au electrodes: the inner pair of exposed areas in contact with the saline water is used for ion sensing and conductivity measurement, and the outer pair of exposed areas serves as contact pads where conductive wires are soldered for power supply and data acquisition. The optical image in Figure 1 shows that the fabricated salinity sensor can be laminated onto a soft PDMS layer as an additional conformal substrate, and can be easily held and bent with two fingers, demonstrating its flexibility, miniaturized size, and ease of integration into future ocean monitoring devices.

For the practical application of salinity sensors in the ocean environment, it is crucial to ensure that the Au electrodes function effectively for a reasonable period of time in seawater which contains approximately 35 g NaCl/L (35 PSU) on average. Although Au is a widely used electrode material due to its outstanding chemical stability and oxidation resistance, the presence of halide ions (Cl- or Br-) in seawater and the applied operation voltage on the electrodes can trigger the electrolysis reaction of Au and accelerate the dissolution of Au electrodes. To prevent such reaction, we employ various electrochemical analysis techniques in this study to investigate the effects of direct current (DC) potential, alternating current (AC) frequency and AC potential on the performance of salinity sensors (will be discussed in the following section). An AC voltage with an amplitude of 0.6 V is identified as the optimal test potential to prevent the damage of the Au electrode and overcome the limitations of DC voltage by oscillating the ions between the electrodes.

The effect of applied DC potentials on the performance of salinity sensors

To determine the optimal voltage for salinity measurement in the ocean environment, the response current of the salinity sensor is measured under voltages of 0-1.5 V using linear sweep voltammetry (LSV) at salinity levels of 30-40 PSU. This electroanalytical method involves sweeping the potential of a working electrode over a defined potential range while measuring the response current (direct current, DC) flowing through the electrodes, which is utilized to identify the reduction-oxidation (redox) electrochemical reactions and to quantify the electroactive species in a solution. **Figure 2A** shows the LSV curves of salinity sensors tested with an applied potential range of 0-1.5 V. At the beginning, the curves under different NaCl concentrations increase very slowly and highly overlap with each other. However, all LSV curves at different salinity levels start rising at 0.8 V (zoom-in curves in Figure 2A), indicating that a redox reaction occurs at this potential. Based on the potential-pH diagram (Pourbaix diagram) of the gold-chloride-water system, which investigates the electrochemical behavior of Au in NaCl solution and plots the theoretical potential of reduction reactions, Au reacts with chloride ions through the following reactions and form $AuCl_4^-$ and $AuCl_2^-$ anions when the potential exceeds 0.8 V.[35, 39]

$$Au+4Cl^- \rightarrow AuCl_4^- + 3e^- \quad E^0(V) = 1.002 - 0.079\log(Cl^-) + 0.0197\log(AuCl_4^-) \qquad (1)$$

$$Au+2Cl^- \rightarrow AuCl_2^- + e^- \quad E^0(V) = 1.15 - 0.1183\log(Cl^-) + 0.0592\log(AuCl_2^-) \qquad (2)$$

These chlorination processes also produce electrons and drive an electric current that corresponds to the rise of LSV current response at 0.8-0.9 V. This clearly explains the reason why the previous research applied a constant AC current of 1 mA on their four-electrode conductivity cell and observed severe damage to the outer pair of Au electrodes.[29] Under their operating conditions, the resulting high resistance of the conductivity sensor (R=1/G > 800 Ω) can lead to the voltage between the two electrodes above 0.8 V (V= 800 Ω × 1 mA), which exceeds the chlorinating potential and cause Au dissolution. Therefore, the optimal condition for salinity measurement is the constant voltage mode below 0.8 V, where the chlorination reactions can be avoided to prevent Au electrodes from corroding and dissolving in NaCl solution. In addition, response currents under different NaCl concentrations become differentiable at an applied potential of above 1.2 V, with the maximum current variations observed at 1.35 V (2.98 μA at 30 PSU and 4.70 μA at 40 PSU), which is consistent with the standard reduction potentials of chlorine/chloride ions (E^0=1.36 V).

Chronoamperometry, a time-dependent current (DC) measurement at steps of constant potential, is then performed to study the kinetics of charge transport at applied voltages below 0.8 V. Here, three steps of constant potential (0.2 V, 0.4 V, and 0.6 V) are applied to the salinity sensor in a 30 PSU NaCl solution and the response current is recorded for 1 min at each step. As shown in the applied voltage-time waveform (**Figure 2B** left y-axis) and response current-time profile (Figure 2B right y-axis), the initial currents for each step are 0.07 μA, 0.15 μA and 0.27 μA, respectively. However, the current drops rapidly and down to below 0.005 μA within 1 minute regardless of the applied voltage value. The sharp decline in current is due to the migration of Na^+ and Cl^- ions, which gradually accumulate near the electrode surfaces, eventually blocking the current flow between the two electrodes. This phenomenon, which is known as the polarization effect, may negatively affect the accuracy of conductivity measurements.[40, 41] According to Ohm's law (R=V/I), the calculated resistance of the salinity sensor would soar from 2.2 MΩ to 122.5 MΩ within 1 minute of testing at the constant voltage of 0.6 V. Consequently, despite solving the issue of electrode damage, applying a DC voltage below 0.8 V is not suitable for salinity measurements because it restricts the mobility of ions and causes significant errors in resistance measurements.

The optical microscope images of the salinity sensor captured before and after LSV measurements confirm that the Au electrodes undergo the electrolysis reactions at a sweeping voltage range of 0–1.5 V. As shown in Figure 2C, one side of the Au electrode is severely corroded and dissolved after test, indicating the chlorination processes occur at the anode terminal and causes the anodic Au dissolution.

The effect of AC frequency on the performance of salinity sensors

To diminish the polarization effect at low DC voltage (<0.8 V), alternating current (AC) is utilized to keep the charged ions oscillating between electrodes. The electrochemical impedance spectroscopy (EIS) is used to evaluate the changes in the impedance (Z), which quantifies the opposition to AC flowing through the circuit, of salinity sensors to determine salinity levels. EIS measures impedance as a complex number with magnitude (|Z|) and phase angle ($\angle\Phi$) by applying low-amplitude AC voltages over a range of frequencies. Purely resistive impedance (Z_R=R) is independent of frequency and has a phase angle of 0°, while purely capacitive impedance (Z_C=1/jωC, ω=2πf) varies with frequency and its phase angle is -90°.

To study the effect of AC frequency on the performance of salinity sensors, the measured impedance magnitude and phase angle are plotted as a function of frequency in **Figure 3 A and 3B**. The impedance of the salinity sensor decreases from approximately 20 kΩ to 100 Ω when the AC frequency increases from 1 kHz to 500 kHz. Most importantly, the impedance curves show a good correlation between impedance values and salinity levels (the lower the salinity, the higher the impedance) at each constant frequency, as shown in the zoom-in view of impedance curves at the frequency of 1 kHz, 10 kHz, and 100 kHz (**Figure 3 I-III**). The relative impedance change ($\Delta Z/Z_0$, %), with Z_0 being the impedance at 30 PSU, is also plotted as a function of salinity levels to compare the sensitivity of the salinity sensor at different frequencies.

Figure 3C shows that the AC frequency has a noticeable effect on the performance of the salinity sensor. Overall, the sensitivity (defined as the absolute value of relative impedance change ($|\Delta Z/Z_0|$) of the salinity sensor is improved as the AC frequency increases from 1 kHz to 500 kHz. At the frequency of 1 kHz, $|\Delta Z/Z_0|$ is approximately 5.5% under a salinity change from 30 PSU to 40 PSU. $|\Delta Z/Z_0|$ increases to 6.9% and 15.8% at 100 kHz and 500 kHz, respectively. Moreover, there is a strong negative correlation between relative impedance changes and phase angles (**Figure S1**). The minimum relative impedance change at 10 kHz corresponds to its maximum phase angles (-83.2°), and the sharply increased relative impedance change at 500 kHz is correlated to its lowest phase angle (-44.4°). According to **Figure 3 A,B**, the magnitude of the impedance varies with frequency, and the phase angles are negative, revealing that the salinity sensor tested in NaCl solution contains both the resistive and capacitive properties. The capacitive behavior of the salinity sensor in the EIS measurements is associated to the double-layer capacitance that associated with two layers of opposing charged ions at the surface of the electrode. Specifically, the polarization effect is not fully eliminated even under the AC conductivity measurement. Various approaches, such as increasing the electrode surface area, applying an appropriate AC frequency, and using a four-electrode cell, have been reported to weaken the negative impact of double-layer capacitance.[40, 41] Please note that these approaches are not the focus of this study and will be studied elsewhere.

The effect of AC voltage and exposed sensing areas on the performance of salinity sensors

Impedance measurements using the low-amplitude AC signal (0.01 V) in Figure 3C have demonstrated the strong linearity between relative impedance changes and salinity levels. In this section, various applied AC voltage and exposed sensing areas are studied to accelerate the ionic transport, reduce the current density, and therefore decrease the influence of double-layer capacitance on the performance of the salinity sensor. According to the impedance values measured at AC voltages of 0.01 V, 0.4 V, 0.6 V and 1.0 V (**Figure 4A**), a higher applied AC voltage leads to a lower impedance of salinity sensors due to the increased ionic mobility and conductivity. **Figure 4B** shows the linear relationship between relative impedance changes and salinity levels under applied AC voltages of 0.01 V-1.0 V. We can see that when being tested under salinity levels of 30 PSU-40 PSU, $|\Delta Z/Z_0|$ of the salinity sensor increases from 6.8% to 52.3% as the applied AC voltage rises from 0.01 V to 1.0V, which is attributed to its decreased phase shift angle and reduced polarization (**Figure S2**). Such results indicate that a larger applied AV voltage could enhance the sensitivity of the salinity sensor. However, as shown in the optical images of salinity sensors before and after salinity measurements (**Figure 4C**), the Au electrodes are damaged under 1.0 V V_{AC} as the chlorination processes are activated at voltages above 0.8 V, which is consistent with the study on the effect of DC voltage on salinity sensors earlier. In addition, the AC signal periodically reverses its direction, causing anodic reactions at both terminals, and corrode both sides of the Au electrode. Conversely, no degradation of Au electrodes is observed when the salinity sensor is tested at 0.6 V V_{AC}. Thus, as long as the voltage is lower than the redox potential of gold chlorination reaction (0.8 V), increasing the applied voltage is an effective approach to increase the sensitivity of the salinity measurement.

We further study the effect of exposed electrode areas on the performance of the salinity sensor using 0.6 V (AC) to avoid Au dissolution. As described earlier, the 4 mm×4 mm electrodes are encapsulated by a parylene C layer, and the exposed sensing areas are defined by patterning the parylene C layer via a reaction ion etching (RIE) process. The exposed widths of the electrode sensing areas are 20 μm, 300 μm, 500 μm and 1000 μm, which are denoted as E20, E300, E500 and E1000, respectively. For example, the E20 salinity sensor has a pair of 20 μm×4 mm exposed regions in contact with the saline solution. **Figure 4D,E** show that a larger exposed area results in lower impedance values under the same salinity level and higher relative impedance changes $|\Delta Z/Z_0|$ over 30-40 PSU. In addition, increasing the exposed area can improve the sensitivity of the salinity sensor, as the resulting lower current densities (**Table S1**) are accompanied with reduced polarization effect. The optical images of salinity sensors in **Figure 4F** show various exposed areas after salinity measurements, confirming that the salinity sensors tested in NaCl solution at 0.6V V_{AC} experience no damage on their Au electrodes.

Performance diagram of salinity sensors and time-dependent AC salinity measurement

To provide guidance for the selection of optimal parameters for testing the Au-based salinity sensors in chloride-containing solutions, we establish a performance diagram by plotting the contour of the sensor sensitivity (defined above as $|\Delta Z/Z_0|$) versus DC/AC voltage and frequency, as shown in **Figure 5A**. The performance diagram is divided into four regions: 1) Gold chlorination (red, observed electrode damage); 2) Polarization effect (blue, $|\Delta Z/Z_0|<5\%$); 3) Low sensitivity (yellow, $|\Delta Z/Z_0|=5\text{-}10\%$); and 4) High sensitivity (green, $|\Delta Z/Z_0|>10\%$). Applying a potential above 0.8 V (DC or AC) to Au electrodes in the presence of Cl^- forms soluble gold-chloride complexes, resulting in dissolution and delamination of the Au thin-film electrodes.[34] In addition to the testing results of Au-based salinity sensors in this study, it has been reported that Au electrodes with a thickness of 300 nm were tested in PBS (pH=7.4), which typically contains ~0.1 M NaCl, at different voltage inputs for chronic neural electrophysiology applications.[34] The lifetime of the electrodes decreased with increasing voltage, with gold dissolution and electrode failures observed after 6 h, 2 h, and 5 min at 2V, 3V, and 5V, respectively.[34] Therefore, the gold chlorination reaction (red region) at voltage greater than 0.8 V needs to be avoided for minimizing damage to the Au electrodes. When tested with DC signals or low-frequency (1kHz and 10kHz) and low-voltage

(0.01 V and 0.3 V) AC signals, the polarization effect (blue region) causes insufficient sensitivity ($|\Delta Z/Z_0|$) of less than 5%. When a DC signal is applied, charged ions accumulate near the electrodes, blocking current flow and significantly increasing the equivalent resistance of the solution.[41] Similarly, an applied AC signal at low frequencies for impedance measurements generates electric double layers due to ion movement to the electrodes under electrostatic forces.[40] The double-layer capacitance can cause voltage/impedance measurement errors that need to be addressed.[40, 41]

Furthermore, the performance diagram shows a high sensitivity (green) region representing sensitivity higher than 10% and a low sensitivity (yellow) region with sensitivity values between 5-10%. The sensitivity can be enhanced by using relatively high frequency and voltage to minimize double-layer effects and capacitance contribution to impedance.[23, 42] In addition to the studies in this work, the performance diagram is also validated in many works. For instance, an Au-electrode conductivity sensor in a sweat collection patch operated at 0.2 Vpp (peak-to-peak voltage) and a frequency of 80 kHz (in the low sensitivity region of diagram) exhibited a conductance sensitivity of 24 μS/ mM in the NaCl solution with a concentration range of 10−150 mM. [42] Another Au-electrode impedance-based sweat sensor, which was operated at 100 kHz with an AC signal amplitude of 400 mV (in the high sensitivity region of diagram), possessed an improved conductance sensitivity of approximately 70 µS/ mM NaCl calculated from the admittance change when the NaCl concentration varies from 15 to 60 mM.[23] The results in this study and those from previous studies effectively validate the performance diagram, which can provide significant guidance for the operation of Au-based electrochemical sensors.

To realize wearable electronic sensors systems for real-time ocean environment monitoring and data transmission, the salinity sensors need to be integrated with electronics that can offer an AC voltage source and record the impedance changes of salinity sensors for salinity measurement. Here, we demonstrate a proof-of-concept study that utilizes a voltage divider circuit, consisting of an input voltage source and two impedances connected in series, which can create an output voltage that is a fraction of the input voltage. The voltage divide ratio is determined by the two impedances and is given by $V_{output}=Z_S/(Z_0+Z_S)\times V_{input}$. Using this basic circuit, the impedance values of salinity sensors at different salinity levels can be converted into output voltage signals for further data processing and recording. In the experimental setup for time-dependent salinity measurements (as described in the experimental section and shown in **Figure 5B**), an input 0.6 V_{RMS} AC (root mean square value of AC voltage) square wave with a frequency of 1 kHz provided by a function generator is applied across the series impedance pair of a constant resistance value of 20 kΩ (Z_0) and a salinity sensor (Z_S). The output voltage signals across the salinity sensor are recorded by an oscilloscope and a digital multimeter. As the salinity level increases from 30 PSU to 40 PSU, the impedance of the salinity sensor decreases, resulting in a decrease in the amplitudes of the output voltage due to the corresponding change in the divide ratio. (**Figure 5C**). Please note that the shape of the output waveforms is not the same as the input square wave due to the capacitive behavior of salinity sensors.

The time-dependent output voltage is recorded under salinity levels ranging from 30 PSU to 40 PSU, and the results are shown in **Figure 5D.** The output voltage decreases as the addition of NaCl solution with higher salinity levels, which is consistent with prior results in Figure 3 and Figure 4. The output voltage drops to a lower value in 5 seconds and stabilizes at a relatively steady voltage within 2 minutes, which is considered as a quick response of the salinity monitoring.[30] In addition, the relationship between relative voltage change ($\Delta V/V_0$, %) and salinity levels presents a good sensitivity ($|\Delta V/V_0|$=~15%) and linearity (R^2=0.99), as shown in **Figure 5E**. For future applications, the output voltage signal will be converted to analog-to-digital (ADC) signals and sent to external computing/recording devices via a Bluetooth module for short-distance testing or an acoustic signal transmitter for deep-sea monitoring.

3. Conclusions

In summary, we develop soft, flexible conductivity sensors and systematically study the effect of the magnitude and frequency of operating voltage and exposed sensing areas on the performance of the sensor. We find that an operating voltage lower than the redox potential of the gold chlorination reaction at approximately 0.8 V can effectively eliminate the chloride-induced corrosion and dissolution of gold-based electrochemical sensors. In addition, an AC signal with relatively high frequency and amplitude (~0.6 V) can reduce the polarization effect and provide better sensitivity than DC or low-frequency and low-amplitude AC signals. A performance diagram is constructed to provide guidance for avoiding gold chlorination and polarization effect and in the meanwhile to identify operating voltage and frequency for high sensitivity. The results provide an important guideline for the development of soft metallic-electrode electrochemical sensors that are used for biosensing or hydro-environmental analysis.

Moreover, a salinity measurement circuit consisting of a 0.6 V AC voltage source, a voltage divider and a salinity sensor has demonstrated high accuracy and quick response time in real-time salinity monitoring. The future prospect of this work includes incorporating soft salinity sensors with other physical sensors like temperature and pressure sensors into a fully functional multimodal sensing system for real-time CTD (conductivity-temperature-depth) monitoring of the ocean environments,[37] as well as integration with other platforms like soft robotics and diver equipment.

4. Experimental Section

Fabrication of soft salinity sensors

The soft salinity sensor comprises of a top encapsulation layer (parylene C, 5 μm), a pair of bilayer chromium (Cr, 10 nm) / gold (Au, 100 nm) thin-film electrodes (each measuring 4mm x 4mm), and soft parylene C (5 μm)/ polyimide (PI, 7.6 μm) substrates. The fabrication processes were reported in previous work[37] and provided as follows. A layer of PDMS (Sylgard 184, Dow, with an elastomer/curing agent weight ratio of 10:1) was spin-coated onto a glass slide at 1500 rpm for 35 s to enhance the adhesion between the subsequent PI substrate and glass. A 7.6 μm thick PI film was then laminated onto the PDMS-coated glass substrate, and a 5 μm parylene C (Specialty Coating Systems Inc.) layer was deposited on top of the PI film. Next, a bilayer of Au (100 nm)/Cr (10 nm) thin film was deposited onto the parylene C layer using a magnetron sputtering system (AJA Orion-8 Magnetron Sputtering System, AJA

International Inc.). The Cr/Au thin film was then patterned into separated electrodes via photolithography and wet-etching technologies. The patterned sensor electrodes were then encapsulated by depositing a top parylene C layer. To define exposed ion sensing areas for salinity sensors, the top parylene C encapsulation layer was patterned by photolithography processes, followed by reactive ion etching (RIE) with oxygen plasma.

Electrochemical measurement of salinity sensors

Saline solution with salinity levels of 30-40 practical salinity unit (PSU, g/kg) for all sensor characterizations were prepared by dissolving 30-40 g of NaCl in deionized (DI) water. Electrochemical measurements were performed using a potentiostat/galvanostat instrument (Autolab PGSTAT128N, Metrohm). Linear sweep voltammetry (LSV) was swept from 0 V to 1.5 V at a scan rate of 0.1 V/s and step of 0.01 V. Chronoamperometry applied three steps of voltage (0.2 V, 0.4 V and 0.6 V) and recorded the respond current at each step for 1 minute with an interval time of 0.1 s. Electrochemical impedance spectroscopy (EIS) was tested in the FRA impedance potentiostatic mode and measured by applying a sinusoidal excitation signal (sine wave) with a frequency from 500 kHz to 1 kHz and an amplitude of 0.01 V_{RMS}. The effect of AC voltage and exposed sensing area on the performance of salinity sensor were performed on a LCR meter (IM3533, Hioki). The LCR meter recorded the impedance values once per second for 1 min for each test condition. The effect of AC voltage (0.01 V, 0.4 V, 0.6 V and 1.0 V) was tested at a constant frequency of 1 kHz with salinity sensors with the same exposed sensing area (uncovered width of 500 μm, denoted as E500). The effect of exposed sensing area of salinity sensors was tested at a constant frequency of 1 kHz and constant applied V_{AC} of 0.6 V.

Voltage divider circuit for time-dependent salinity measurement

A function generator (SDG1032X, Siglent) was used to generate a square wave AC voltage with an amplitude of 0.6 V_{RMS} (root mean square value of AC voltage) and a frequency of 1 kHz. This input voltage was applied across a programmable resistor board set at a constant resistance value of 20 kΩ (Z_0) and a salinity sensor (Z_S) that were connected in series. The output voltage waveforms across the salinity sensor were captured using an oscilloscope (DS1104Z Plus, Rigol). To test the time-dependent salinity measurement, different concentrations of NaCl were added to the solution to achieve salinity levels of 30-40 PSU. The output AC voltage was continuously measured by a digital multimeter (34470A, Keysight) in V_{RMS} values. The digital multimeter was operated in data logging mode to record the AC voltage every second.

Author Contributions

X.W. conceived the idea and supervised the experiments. S.L. conducted the experiments on the fabrication and testing of salinity sensors. Y.L. assisted with the experiments. X.W. and S.L. wrote the manuscript. All authors discussed and commented on the manuscript.

Conflicts of interest

There are no conflicts to declare.

Acknowledgements

S.L., Y.L., and X.W. would like to acknowledge the support from the Office of Naval Research (N00014-19-1-2688 and N00014-21-1-2342). In addition, this work made use of the maskless aligner μMLA, which was funded by the Defense University Research Instrumentation Program from the Office of Naval Research (N00014-21-1-2223).

References

1. M. Lin, Z. Zheng, L. Yang, M. Luo, L. Fu, B. Lin and C. Xu, *Adv. Mater.*, 2022, **34**, e2107309.
2. G. Su, S. Yin, Y. Guo, F. Zhao, Q. Guo, X. Zhang, T. Zhou and G. Yu, *Mater Horiz*, 2021, **8**, 1795-1804.
3. I. Heck, W. Lu, Z. Wang, X. Zhang, T. Adak, T. Cu, C. Crumley, Y. Zhang and X. S. Wang, *Advanced Materials Technologies*, 2022, **8**.
4. T. Leelasree, V. Selamneni, T. Akshaya, P. Sahatiya and H. Aggarwal, *J Mater Chem B*, 2020, **8**, 10182-10189.
5. D. H. Keum, S. K. Kim, J. Koo, G. H. Lee, C. Jeon, J. W. Mok, B. H. Mun, K. J. Lee, E. Kamrani, C. K. Joo, S. Shin, J. Y. Sim, D. Myung, S. H. Yun, Z. Bao and S. K. Hahn, *Sci Adv*, 2020, **6**, eaba3252.
6. Q. Chen, Z. Chen, D. Liu, Z. He and J. Wu, *ACS Appl Mater Interfaces*, 2020, **12**, 17713-17724.

7. A. Scidà, S. Haque, E. Treossi, A. Robinson, S. Smerzi, S. Ravesi, S. Borini and V. Palermo, *Mater. Today*, 2018, **21**, 223-230.
8. Y. Zhao, B. Wang, H. Hojaiji, Z. Wang, S. Lin, C. Yeung, H. Lin, P. Nguyen, K. Chiu, K. Salahi, X. Cheng, J. Tan, B. A. Cerrillos and S. Emaminejad, *Sci Adv*, 2020, **6**, eaaz0007.
9. Z. Pu, X. Zhang, H. Yu, J. Tu, H. Chen, Y. Liu, X. Su, R. Wang, L. Zhang and D. Li, *Sci Adv*, 2021, **7**.
10. O. Parlak, S. T. Keene, A. Marais, V. F. Curto and A. Salleo, *Sci Adv*, 2018, **4**, eaar2904.
11. Y. Park, C. K. Franz, H. Ryu, H. Luan, K. Y. Cotton, J. U. Kim, T. S. Chung, S. Zhao, A. Vazquez-Guardado, D. S. Yang, K. Li, R. Avila, J. K. Phillips, M. J. Quezada, H. Jang, S. S. Kwak, S. M. Won, K. Kwon, H. Jeong, A. J. Bandodkar, M. Han, H. Zhao, G. R. Osher, H. Wang, K. Lee, Y. Zhang, Y. Huang, J. D. Finan and J. A. Rogers, *Sci Adv*, 2021, **7**.
12. S. H. Ko, S. W. Kim and Y. J. Lee, *Sci Rep*, 2021, **11**, 21101.
13. R. Hajian, S. Balderston, T. Tran, T. deBoer, J. Etienne, M. Sandhu, N. A. Wauford, J. Y. Chung, J. Nokes, M. Athaiya, J. Paredes, R. Peytavi, B. Goldsmith, N. Murthy, I. M. Conboy and K. Aran, *Nat Biomed Eng*, 2019, **3**, 427-437.
14. J. Sabate Del Rio, H. K. Woo, J. Park, H. K. Ha, J. R. Kim and Y. K. Cho, *Adv. Mater.*, 2022, **34**, e2200981.
15. H. Liu, A. Yang, J. Song, N. Wang, P. Lam, Y. Li, H. K. Law and F. Yan, *Sci Adv*, 2021, **7**, eabg8387.
16. Y. Gao, D. T. Nguyen, T. Yeo, S. B. Lim, W. X. Tan, L. E. Madden, L. Jin, J. Y. K. Long, F. A. B. Aloweni, Y. J. A. Liew, M. L. L. Tan, S. Y. Ang, S. D. Maniya, I. Abdelwahab, K. P. Loh, C. H. Chen, D. L. Becker, D. Leavesley, J. S. Ho and C. T. Lim, *Sci Adv*, 2021, **7**.
17. R. Li, H. Qi, Y. Ma, Y. Deng, S. Liu, Y. Jie, J. Jing, J. He, X. Zhang, L. Wheatley, C. Huang, X. Sheng, M. Zhang and L. Yin, *Nat Commun*, 2020, **11**, 3207.
18. M. Ku, J. Kim, J. E. Won, W. Kang, Y. G. Park, J. Park, J. H. Lee, J. Cheon, H. H. Lee and J. U. Park, *Sci Adv*, 2020, **6**, eabb2891.
19. H. P. Phan, Y. Zhong, T. K. Nguyen, Y. Park, T. Dinh, E. Song, R. K. Vadivelu, M. K. Masud, J. Li, M. J. A. Shiddiky, D. Dao, Y. Yamauchi, J. A. Rogers and N. T. Nguyen, *ACS Nano*, 2019, **13**, 11572-11581.
20. H. Lee, C. Song, Y. S. Hong, M. Kim, H. R. Cho, T. Kang, K. Shin, S. H. Choi, T. Hyeon and D. H. Kim, *Sci Adv*, 2017, **3**, e1601314.
21. J. Xu, Z. Zhang, S. Gan, H. Gao, H. Kong, Z. Song, X. Ge, Y. Bao and L. Niu, *ACS Sens*, 2020, **5**, 2834-2842.

22. Y. Song, J. Min, Y. Yu, H. Wang, Y. Yang, H. Zhang and W. Gao, *Sci Adv*, 2020, **6**.
23. H. Y. Y. Nyein, L.-C. Tai, Q. P. Ngo, M. Chao, G. B. Zhang, W. Gao, M. Bariya, J. Bullock, H. Kim, H. M. Fahad and A. Javey, *ACS Sensors*, 2018, **3**, 944-952.
24. Y. H. Kim, K. Lee, H. Jung, H. K. Kang, J. Jo, I. K. Park and H. H. Lee, *Biosens. Bioelectron.*, 2017, **98**, 473-477.
25. P. K. Vabbina, A. Kaushik, N. Pokhrel, S. Bhansali and N. Pala, *Biosens. Bioelectron.*, 2015, **63**, 124-130.
26. H. Teymourian, C. Moonla, F. Tehrani, E. Vargas, R. Aghavali, A. Barfidokht, T. Tangkuaram, P. P. Mercier, E. Dassau and J. Wang, *Anal. Chem.*, 2020, **92**, 2291-2300.
27. S. F. Shaikh, H. F. Mazo-Mantilla, N. Qaiser, S. M. Khan, J. M. Nassar, N. R. Geraldi, C. M. Duarte and M. M. Hussain, *Small*, 2019, **15**, e1804385.
28. A. Kaidarova, M. A. Khan, M. Marengo, L. Swanepoel, A. Przybysz, C. Muller, A. Fahlman, U. Buttner, N. R. Geraldi, R. P. Wilson, C. M. Duarte and J. Kosel, *npj Flexible Electronics*, 2019, **3**.
29. A. Kaidaorva, M. Marengo, G. Marinaro, N. R. Geraldi, R. Wilson, C. M. Duarte and J. Kosel, *Results in Materials*, 2019, **1**.
30. J. M. Nassar, S. M. Khan, S. J. Velling, A. Diaz-Gaxiola, S. F. Shaikh, N. R. Geraldi, G. A. Torres Sevilla, C. M. Duarte and M. M. Hussain, *npj Flexible Electronics*, 2018, **2**.
31. F. Akhter, H. R. Siddiquei, M. E. E. Alahi, K. P. Jayasundera and S. C. Mukhopadhyay, *IEEE Internet of Things Journal*, 2022, **9**, 14307-14316.
32. M. Chen, M. Zhang, X. Wang, Q. Yang, M. Wang, G. Liu and L. Yao, *Sensors (Basel)*, 2020, **20**.
33. Y. Sui and C. A. Zorman, *J. Electrochem. Soc.*, 2020, **167**.
34. J. Li, E. Song, C. H. Chiang, K. J. Yu, J. Koo, H. Du, Y. Zhong, M. Hill, C. Wang, J. Zhang, Y. Chen, L. Tian, Y. Zhong, G. Fang, J. Viventi and J. A. Rogers, *Proc Natl Acad Sci U S A*, 2018, **115**, E9542-E9549.
35. O. Kasian, N. Kulyk, A. Mingers, A. R. Zeradjanin, K. J. J. Mayrhofer and S. Cherevko, *Electrochim. Acta*, 2016, **222**, 1056-1063.
36. N. Ali, J. A. Teixeira, A. Addali, M. Saeed, F. Al-Zubi, A. Sedaghat and H. Bahzad, *Materials (Basel)*, 2019, **12**.
37. Y. Li, G. Wu, G. Song, S. H. Lu, Z. Wang, H. Sun, Y. Zhang and X. Wang, *ACS Sens*, 2022, **7**, 2400-2409.
38. A. Kaidarova, M. Marengo, G. Marinaro, N. Geraldi, C. M. Duarte and J. Kosel, *Advanced Materials Interfaces*, 2018, **5**.
39. G. H. Kelsall, N. J. Welham and M. A. Diaz, *J. Electroanal. Chem.*, 1993, **361**,

13-24.

40. J. Park, W.-M. Choi, K. Kim, W.-I. Jeong, J.-B. Seo and I. Park, *Scientific Reports*, 2018, **8**, 264.
41. B. You, Y. Yue, M. Sun, J. Li and D. Jia, *Sensors (Basel)*, 2021, **21**.
42. A. S. M. Steijlen, K. M. B. Jansen, J. Bastemeijer, P. J. French and A. Bossche, *Anal. Chem.*, 2022, **94**, 6893-6901.

Figures

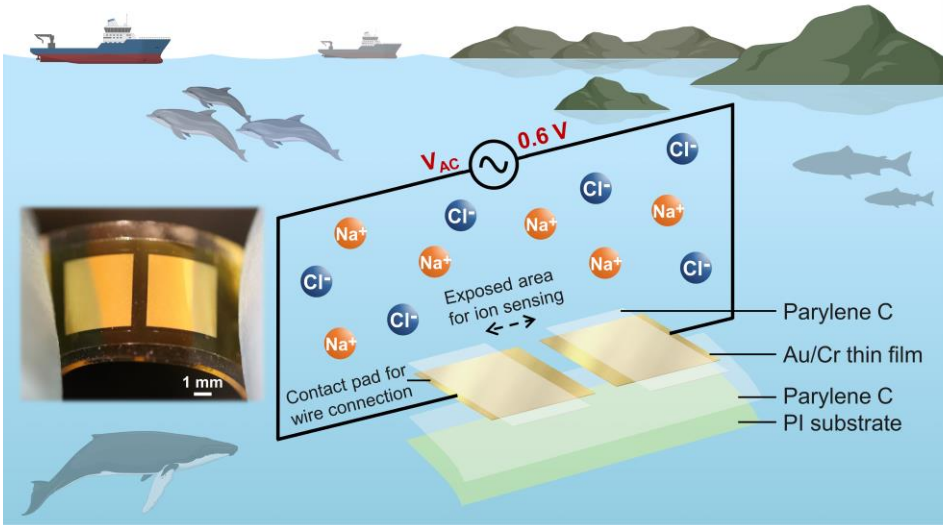

Figure 1. Schematic illustration of the layout and working principle of soft salinity sensors, as well as optical image of a flexible salinity sensor laminated onto a soft PDMS substrate. Created with BioRender.com

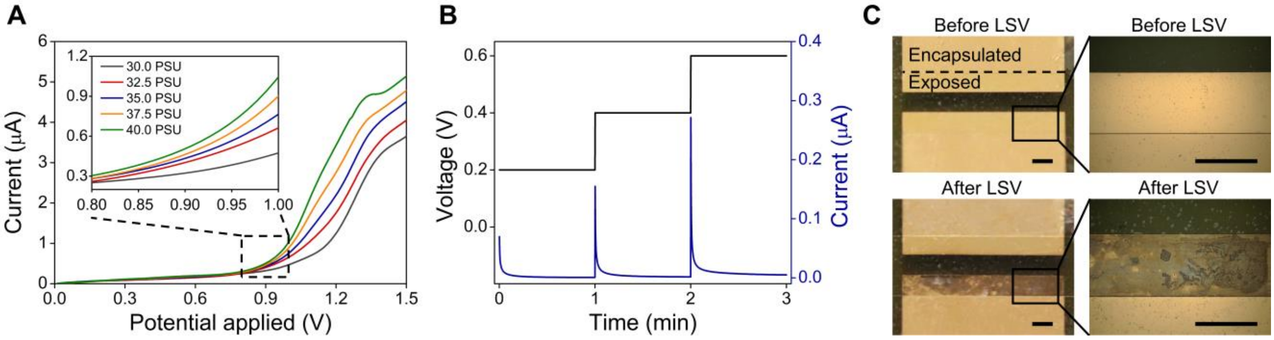

Figure 2. (A) Linear sweep voltammetry (LSV) curves of salinity sensors measured in NaCl solutions at salinity levels of 30-40 PSU. (B) Applied voltage-time waveform and response current-time profile measured by chronoamperometry at a salinity of 30 PSU. (C) Optical images of the salinity sensor before and after LSV measurements scanned in the potential range of 0-1.5 V. Scale bars: 500 μm.

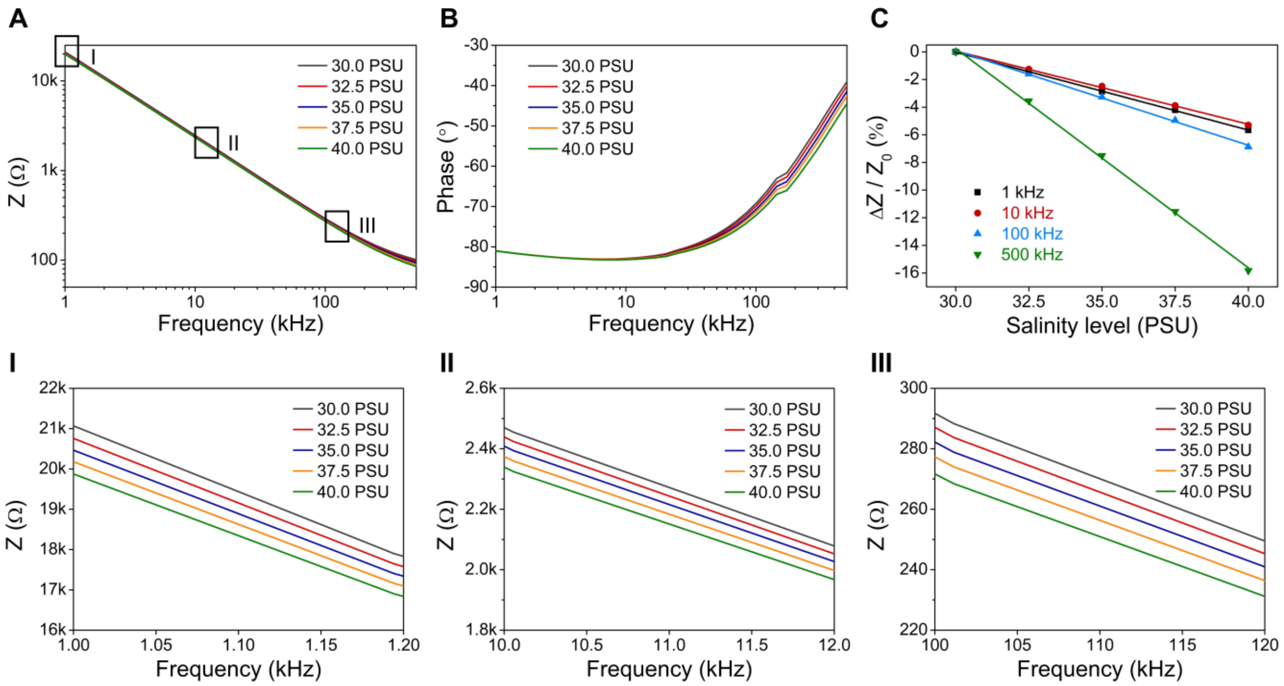

Figure 3. Electrochemical impedance spectroscopy (EIS) curves of salinity sensors with an exposed sensing area of 500 μm tested in NaCl solution at salinity levels of 30-40 PSU. (A) Impedance as a function of frequency in range of 1-500 kHz. Zoom-in EIS curves at frequency of (I) 1-1.2 kHz, (II) 10-12 kHz and (III) 100-120 kHz. (B) Phase angle as a function of frequency in range of 1-500 kHz. (C) Relative impedance change (ΔZ/Z₀, %) as a function of salinity level at different applied frequency.

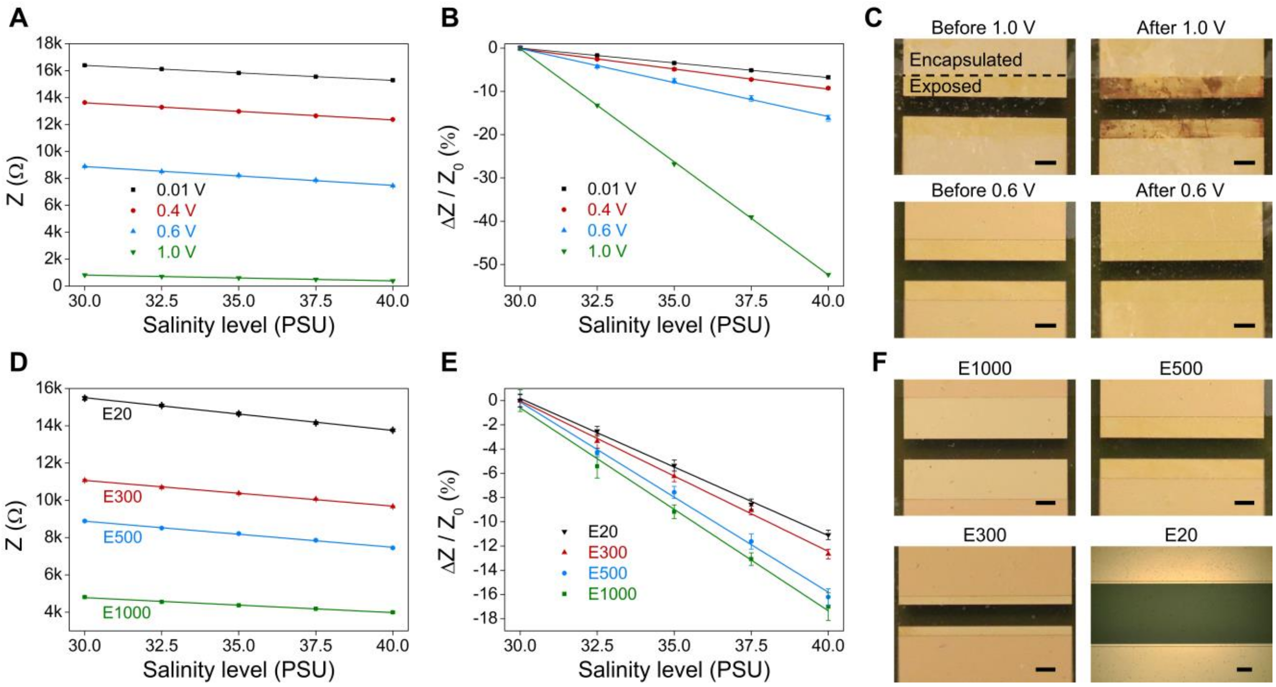

Figure 4. Calibration curves of (A) impedance value and (B) relative impedance

change ($\Delta Z/Z_0$, %) at different applied V_{AC} values as a function of salinity level (salinity sensors with the same exposed sensing area of 500 μm tested at a constant frequency of 1 kHz). (C) Optical images of salinity sensors before and after salinity measurements at applied AC voltage of 1.0 V and 0.6 V. Scale bars: 500 μm. Calibration curves of (D) impedance value and (E) relative impedance change (ΔZ/Z0, %) for salinity sensors of various exposed sensing areas as a function of salinity levels (tested at constant frequency of 1 kHz and constant applied V_{AC} of 0.6 V). (F) Optical images of salinity sensors with various exposed sensing area after salinity measurements. Scale bars: 100 μm for the microscopic image of E20; 500 μm for the rest of the images.

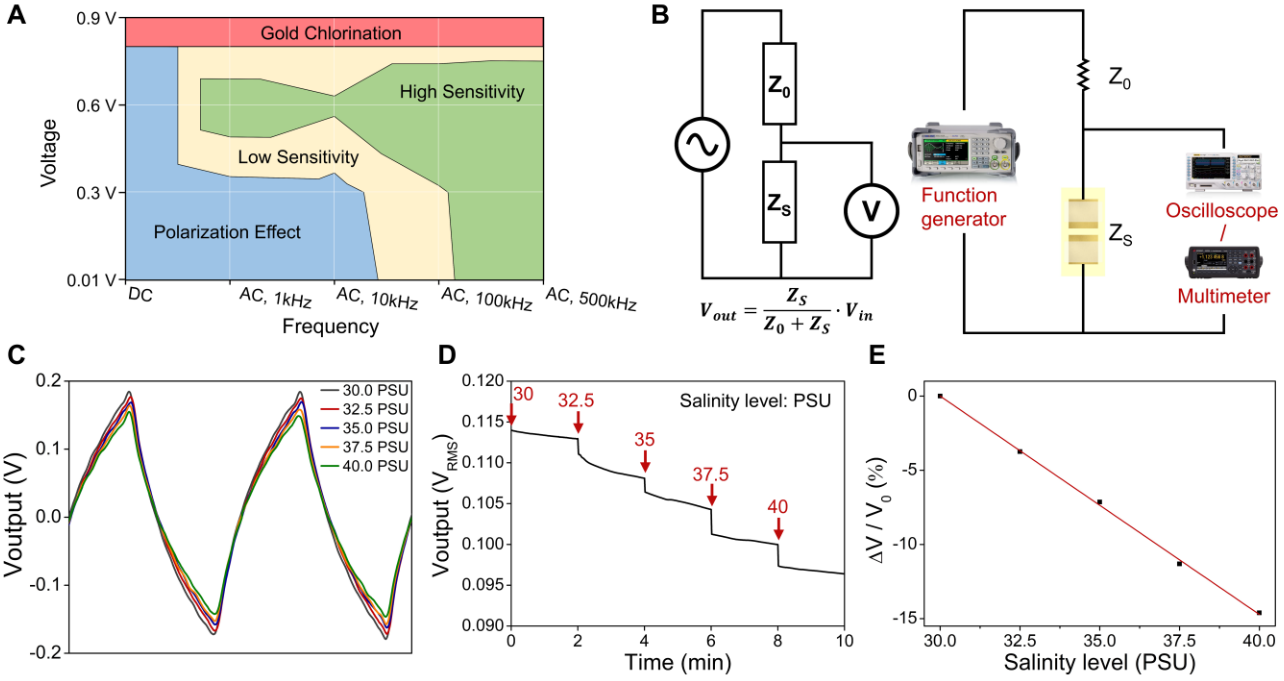

Figure 5. (A) Performance diagram of gold-based salinity sensors operated at various DC/AC voltage and frequency. (B) Voltage divider circuit and experimental setup for time-dependent salinity measurements. (C) Output AC waveforms of the salinity sensor recorded from an oscilloscope at salinity levels of 30-40 PSU. (D) Time-dependent output voltage (V_{RMS}) recorded from a digital multimeter at salinity levels of 30-40 PSU. (E) Calibration curve of relative output voltage change ($\Delta V/V_0$, %) of the salinity sensor as a function of salinity levels.